Mapping Three-Dimensional Tumor Heterogeneity through Deep Learning Inference of Spatial Transcriptomics from Routine Histopathology: A Proof-of-Concept Comparative Study

Zarif L. Azher* ZAZHER@CALTECH.EDU
California Institute of Technology, USA
Cedars-Sinai Medical Center, USA

Gokul Srinivasan GOKUL.SRINIVASAN.23@DARTMOUTH.EDU
Keluo Yao KELUO.YAO@CSHS.ORG
Minh-Khang Le KHANG.STUDENTOFMEDICINE@GMAIL.COM
Cedars-Sinai Medical Center, USA

Ken S. Lau KEN.S.LAU@VANDERBILT.EDU
Harsimran Kaur HARSIMRAN.KAUR@VANDERBILT.EDU
Vanderbilt University, USA

Fred Kolling FRED.W.KOLLING.IV@DARTMOUTH.EDU
Louis Vaickus LOUIS.J.VAICKUS@HITCHCOCK.ORG
Xiaoying Lu XIAOYING.LIU@HITCHCOCK.ORG
Dartmouth-Hitchcock Medical Center, USA

Joshua J. Levy JOSHUA.LEVY@CSHS.ORG
Cedars-Sinai Medical Center, USA
Dartmouth-Hitchcock Medical Center, USA

Abstract

Spatial transcriptomics (ST) technologies enable the mapping of gene and protein abundance within specific tissue architectures, representing a significant advancement over conventional bulk analyses that can obscure critical prognostic markers tied to spatial contexts. Expanding these analyses to three dimensions (3D) can further uncover intricate biomolecular phenomena that may be truncated or missed in two-dimensional (2D) studies. However, the widespread application of 3D ST profiling is limited by high costs and logistical challenges. Deep learning-based inference of ST data from routine histopathological staining offers a cost-effective alternative, allowing for the exploration of histologically associated biological pathways in 3D and enhancing our ability to detect structures linked to tumor progression. In this proof-of-concept study, we employed deep learning models to infer ST data from routine histopathology for 10 colorectal cancer patients, with 10 serial sections analyzed per patient. Our downstream analyses revealed several key instances where 3D approaches provided enhanced insights into cellular phenomena compared to traditional 2D methods. These findings lay the groundwork for future research aimed at leveraging these methods to investigate subtle 3D biomarkers associated with tumor metastasis and recurrence.

Keywords: pathology, spatial transcriptomics, deep learning, 3D spatial transcriptomics, graph deep learning

Data and Code Availability Data utilized in this study included: 1) Serial histopathological sections of colorectal cancer tissue specimens from the *Dartmouth Hitchcock Medical Center. 2) 10x Genomics Visium Spatial Transcriptomics samples collected and assayed from colorectal cancer patients at the Dartmouth Hitchcock Medical Center. 3) Single-cell RNA sequencing assayed at the Dartmouth Hitchcock Medical Center. We are unable to make data immediately publicly accessible due to institutional restrictions surrounding patient data privacy, though anonymized access can be granted upon reasonable request. The code used to perform anal-

* Corresponding Author

yses in this study is available on the study Github repository.

Institutional Review Board (IRB) Human Research Protection Program IRB of Dartmouth Health gave ethical approval for this work.

1. Introduction

1.1. Spatial Profiling of the Tumor Microenvironment

The highly heterogenous tumor microenvironment (TME) represents a dynamic molecular landscape which shapes tumorigenesis, progression, prognosis, and treatment response (Dagogo-Jack and Shaw; Lüönd et al.; Molinari et al.). Bulk tissue analysis can often overlook relevant and crucial alterations to specific TME components, warranting a spatial analysis which can localize findings to specific tissue architectures and lineages. In recent years, the advent and rising popularity of spatial transcriptomics (ST), which can spatially map high dimensional gene expression across tissue samples, has the potential to significantly enhance our study of tumor heterogeneity by enhancing the scope and range of considered biological pathways. Thus, this technology serves as a broad discovery tool that can facilitate further research optimizing personalized medicine and improved understanding of tumor pathology (Tian et al.).

1.2. The Promise of 3D Pathology

Advances in computation – specifically deep learning approaches - and their application to histopathology have greatly enabled the study of tumors within complex 3D tissue volumes in contrast to traditional pathology assessments conducted on 2D tissue slices (Liu et al.). For instance, Xie et al. segmented prostate glands from 3D biopsy imaging using deep learning and extracted interpretable shape-based features correlated with prognosis that were found to be superior to typical 2D analysis. In a separate work, Lin et al. found that histologic features commonly studied in 2D in fact form complex 3D structures with associated molecular gradients tied to specific tumor phenotypes. Application of these technologies to novel 3D open-top light-sheet microscopy tools may further spur innovation in this field (Glaser et al.).

Recently, methods to resolve ST in 3D have emerged, such as Open-ST, a relatively low-cost sequencing technology tailored for 3D experimentation (Schott et al.). Alternative approaches have applied 2D ST sequencing on serial slices using technologies such as the 10x Genomics Visium Platform, followed by slice integration to generate 3D gene expression models (Vickovic et al.; Wang et al., b,c). These works have demonstrated that ST can reconstruct 3D histological structures and elucidate key molecular underpinnings of relevant tissue morphology (Waylen et al.). Further exploration of 3D ST has the potential to define clinically relevant cancer subtypes and illuminate specific 3D biomolecular pathways that influence tumor progression and prognosis. This approach offers a novel avenue for cancer patient stratification, enabling more precise phenotyping and the identification of new therapeutic targets.

Existing 3D ST methods are typically limited by their need for manual laboratory assaying which often requires high resource cost and processing time, limiting the potential to perform 3D spatial molecular profiling at scale. To mitigate this issue for 2D ST analysis, various works have successfully applied deep learning to infer spatial gene expression from routine histopathological tissue images (Fatemi et al.; Levy-Jurgenson et al.; Zeng et al.). Although some approaches have extended this inference to 3D by extrapolating ST data to serially imaged tissue sections, they still rely on initial ST profiling of the top section and require hematoxylin and eosin (H&E) whole slide images (WSI) taken with identical quality as the serial sections, which has proven challenging. However, to date, no published study has explored or compared 3D ST through the inference of gene expression solely from imaging of underlying tissue collected from serial deeper sections. Such efforts may provide a rapid and low-cost method for researchers and clinicians to assess tumors in high resolution with maximal tissue and molecular context.

1.3. Contributions

Here, we apply a previously developed deep learning model to infer spatial transcriptomics from routine cancer histopathology to serial tissue slices. We use the inferred gene expression profiles to create 3D ST models of tumors, and demonstrate that considering 3D transcriptomic information yields richer understanding of the heterogeneous tumor microenvironment compared to analyzing corresponding 2D slices.

We conduct our study using samples from patients diagnosed with colorectal cancer, a leading cancer causing massive global burden with nearly 2 million annual cases reported (Morgan et al.). Our results suggest that deep learning-driven inference of spatial transcriptomics can help facilitate the transition toward a 3D comprehension of cancer tumors, enhancing both disease understanding and treatment options.

2. Materials and Methods

2.1. Data Acquisition

2.1.1. ST Cohort for Model Training and Internal Validation/Tuning

ST data was collected from 45 pT3 colorectal cancer (CRC) tissue resection specimens using the 10X Genomics Visium CytAssist Platform. These patients varied by their microsatellite instability and metastasis (N/M-stage) status, age, sex, tumor location, grade, and so forth. Visium data preprocessing and quality control was conducted using the SpaceRanger software, resulting in approximately 300,000 total ST spots measuring expression for 17456 genes each. Due to computational constraints and feasibility of this pilot experiment, only the top 1000 most spatially variable genes (SVG) were considered, as identified using the SpatialDE Python package (Svensson et al.). H&E-stained WSI at 40x magnification was also obtained for the same ST samples and co-registered via the CytAssist platform.

2.1.2. Validation Cohort for 3D Inference

Separately, 10 independent CRC tissue specimens were selected for 3D profiling – local/distant tumor involvement was noted for half of these patients. A total of 10 serial sections were performed from each tissue block, with a vertical slice separation distance of 5 microns. Tissue staining and imaging followed the aforementioned protocol (automated tissue staining, imaging with 40X Leica Aperio GT450 scanner) to ensure consistency with what was done for Visium profiling. An adjacent section placed above tissue sections selected for genomics and imaging was annotated by two board-certified pathologists, partitioning the tissue into various histological architectures (e.g., normal epithelium, tumor, tertiary lymphoid structures). WSI representing serial sections from each tissue block were coregistered to form a 3D structure using the VALIS software (Gatenbee et al.).

Finally, we collected a reference single-cell RNA sequencing dataset (scRNASeq) spanning approximately 115,000 cells across 10 patients at serial tissue sections representative of our spatial cohort. Cell-type annotation was performed using the scvi Python package (Lopez et al.) and the Human Colorectal Cancer Atlas (Pelka et al.) reference database for the following types of cells: B cells, epithelial cells, mast cells, myeloid cells, plasma cells, stromal cells, and T cells, natural killer cells, and innate lymphoid cells (TNKILC).

All samples were collected from the Dartmouth Hitchcock Medical Center following appropriate IRB approval. H&E images were stain-normalized using the Macenko method (Macenko et al.). All WSI were split into non-overlapping patches of 512x512 pixels excluding image background. Patches from WSI with corresponding ST available were spatially centered on Visium ST spots.

2.2. Generation of Inferred 3D Spatial Transcriptomics Information

The primary focus of this work is the innovative application of a validated Swin Transformer model to 3D histopathological data, with the goal of gaining new insights into 3D spatial transcriptomics. The Swin Transformer learns meaningful relationships across scales within the input 512x512 images, which is advantageous due to the inherent multi-scale nature of histopathology where macro and micro-architectural features are observable at different levels. Building on a previous study (Fatemi et al.), this new model was designed to predict gene expression profiles from histopathological image patches using a much larger dataset of about 300,000 Visium spots, achieving a median Spearman correlation of 0.55 across the top 1000 SVG. While detailed model development and performance statistics are discussed in a contemporaneous paper currently under review (Srinivasan et al.), validation statistics were presented in this section to demonstrate the model's robustness and readiness for this 3D application. This study leverages the model's capabilities, not as an end, but as a tool to explore and understand the complexities of 3D tissue architecture and gene expression.

The trained ST inference model was applied to tissue image patches from all 2D serial sections. This resulted in an Nx1000 dimensional gene expression

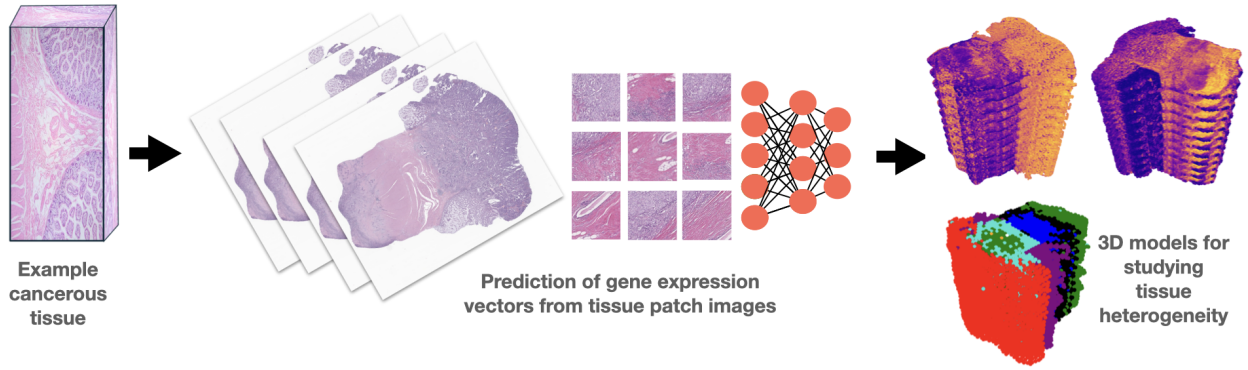

Figure 1: Study workflow overview, including collection of serial 2D images from tumor resections, inference of spatial transcriptomics profiles from image patches using deep learning, and 3D tissue models for studying molecular heterogeneity.

array for each section from each tissue block, where N is the number of patches in that section. For each tissue block, the sections and corresponding inferred ST spots were vertically stacked using VALIS to create 3D ST data representing the captured tumor region. Mean neighborhood pooling on 2D sections were used to average inferred expression from adjacent patches to address downstream computational methods which were infeasible with the near-single cell resolution of the inferred 3D ST data. To enrich 3D ST data with maximum molecular context, we applied the Stitch3D framework (Wang et al., a), which uses graph neural networks (GNN) to learn informative representations of 3D ST where cross-slice information is integrated and slice-wise batch effects are removed. We ensured the removal of these batch effects by visualizing expression profiles colored by slice number using UMAP (McInnes et al.) (Appendix **??**).

2.3. Investigation of Tumor Heterogeneity in 3D

To assess how our 3D ST models enable the investigation of tumor heterogeneity, we first applied the Leiden community detection algorithm (Traag et al.) to the 3D gene expression graphs for spatial domain identification, revealing spatially defined biologically meaningful and coherent regions. Leiden clustering was done at varying resolutions to determine increasingly nuanced and granular clusters. 3D models of identified clusters were visualized for assessment of spatial coherency. Separately, we applied the same algorithm to the ST profile of the tissue slice at the top of each 3D model, both with and without enrichment by Stitch3D (described in previous section). This allowed us to compare detected heterogeneity when full 3D information is used with across all tissue sections within a sample, when 2D analyses are performed after enrichment with 3D information ("2.5D"), and when solely "raw" 2D ST data is used. The consideration of these settings facilitates the nuanced understanding of benefits and drawbacks of typical 2D ST ("Raw 2D"), enriching 2D sections with information from neighboring sections ("2.5D"), and enriching 2D sections with neighboring information while considering all sections together ("3D"). At each resolution, the average number of spatial domains identified by each method across specimens were assessed and compared through calculating a 95% confidence interval.

Next, we used the popular Calinski-Harabasz score (Calinski and Harabasz) (CH score) to compare the clustering quality of 2D vs 3D spatial domains. This metric was selected because it balances cluster separation and distance to assign higher values to well-defined and distinct clusters. The mean CH score across samples was measured and plotted for spatial domains with Leiden resolution ranging from 0.05 to 0.95. Similarly, agreement with ground truth pathology annotations was assessed by measuring and plotting the Fowlkes-Mallow Index (Fowlkes and Mallows) across the same range of Leiden resolutions.

Here, the comparison was between "2.5D" and "Raw 2D " samples, as groundtruth pathology annotations were performed on single 2D image slices.

Finally, we utilized the ability of Stitch3D to estimate spot-level cell-type proportions. Briefly, Stitch3D utilizes the scRNA reference dataset to identify marker genes for each cell-type, and scores the presence of these marker genes in ST spots to deconvolve the relative abundance of each cell-type. Cell-type distributions were visualized in 3D models and qualitatively analyzed for concordance with identified 3D spatial domains. We hypothesized that 3D spatial domains would partially reflect local cellular aggregates of specific lineages, such as tertiary lymphoid structures. To test this hypothesis, we selected example spatial domains which appeared visually concordant with tested cell-types, and determined their top 50 marker genes using Wilcoxon tests. We then used the Enrichr (Kuleshov et al.) tool to explore biological pathways associated with these genes, aiming to determine whether the identified spatial domains correspond to functionally specific cell subtypes. Given the expectation that 2D spatial domains are likely to be more non-specific, we anticipated that these domains would further subdivide in 3D, revealing more nuanced biological pathways. The Reactome Pathway Database (Milacic et al.) was used for the pathway analysis. We also conducted a comparative analysis between broader 2D ST domains and the pathways identified within corresponding subdivisions of these domains based on 3D projections into 2D. This comparison allowed us to evaluate whether the added dimensionality in 3D provides more biologically salient insights into the underlying cellular and molecular structures.

3. Results

3.1. 3D Spatial Transcriptomics Enriches Coherent Spatial Domain Identification

Using the Leiden algorithm, we compared the average number of spatial domains identified when considering corresponding 2D slices ("Raw 2D"), 2D slices enriched with information from 3D models ("2.5D"), and full 3D ST models ("3D"). Consideration of full 3D ST information consistently yielded the greatest number of identified spatial domains across tested resolutions (Table 1) – different domains were relevant to different subsets of 2D serial sections. For each Leiden clustering resolution (0.2, 0.5, 0.8), 3D ST models yielded an average increase in spatial domain count of 71.1%, 92.4%, and 99%, respectively, compared to the top 2D method.

Next, we visualized 3D spatial domains across samples to ensure their histological coherency and qualitative clustering quality. Examples of this analysis are presented in Figure 4. A certified pathologist confirmed that 3D spatial domains were consistent with histological structures of representative section.

Table 1: Tumor heterogeneity measured by average number of spatial domains identified from corresponding 2D and 3D spatial transcriptomics models.

Leiden Resolution	Raw 2D	2.5D	3D
0.2	4.50 ± 0.77	4.40 ± 0.50	7.70 ± 1.88
0.5	7.30 ± 0.76	7.90 ± 0.98	15.20 ± 2.56
0.8	10.10 ± 0.98	10.60 ± 1.38	21.10 ± 3.73

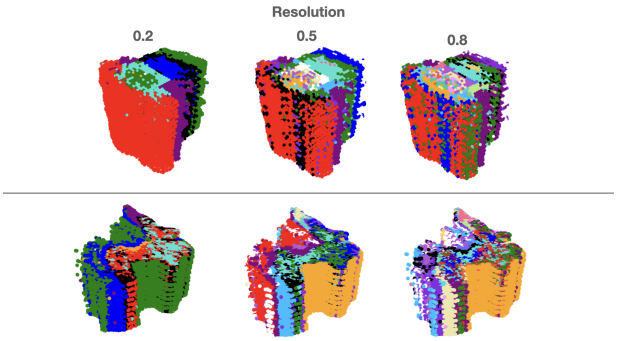

Figure 2: Examples of spatial domains identified in 3D tumor models across tested clustering resolutions.

Spatial domain quality measured by Calinski-Harabasz (CH) scores and agreement with pathology elucidated through Fowlkes-Mallows (FM) scores are presented in Figure 3A. 3D spatial domain clusters were found to be consistently more well-separated and dense measured using CH score across Leiden resolutions. Agreement with histological annotations were similar for "2.5D" and "Raw 2D" samples, illustrating that a 3D GNN did not significantly enhance clustering for the same section but rather clustering

across multiple sections (3D) was more informative. However, the peak FM score for "2.5D" samples was markedly higher than that of "Raw 2D" (53.4 and 49.1, respectively), demonstrating that 3D GNN integration enhanced identification of broader tissue domains.

3.2. Prognostic Cell-Types Localized in 3D vs. 2D

Table 2: Pathway analysis results for 3D and 2D stromal domains.

3D Stromal Domain A	**P-value**	**2D Stromal Domain A**	**P-value**
Metabolism Of Lipids (R-HSA-556833)	4.8e-3	Zinc Efflux And Compartmentalization By SLC30 Family (R-HSA-435368)	3.5e-3
Cholesterol Biosynthesis (R-HSA-191273)	1.3e-2	Trafficking And Processing Of Endosomal TLR (R-HSA-1679131)	6.5e-3
Molecules Associated With Elastic Fibres (R-HSA-2129379)	1.4e-2	Zinc Transporters (R-HSA-435354)	8.5e-3
3D Stromal Domain B		Metal Ion SLC Transporters (R-HSA-425410)	1.3e-2
Signaling By BMP (R-HSA-201451)	1.3e-2	NOTCH3 Intracellular Domain Regulates Transcription (R-HSA-9013508)	1.3e-2
Regulation Of Necroptotic Cell Death (R-HSA-5675482)	1.4e-2	Insulin Processing (R-HSA-264876)	1.3e-2
RIPK1-mediated Regulated Necrosis (R-HSA-5213460)	1.5e-2	Signaling By BMP (R-HSA-201451)	1.3e-2

We visualized estimated relative abundances of prognostic cell-types in our 3D and 2D tumor models from the same samples. Specifically, we investigated T cells, NK cells, and innate lymphoid cells (TNKILC), as well as stromal cell abundances as their presence and spatial distributions were easier to validate visually, and both immune infiltration and collagen remodeling are highly relevant studying CRC progression (Zheng et al.; Zhou et al.). In the tested examples, tissue regions with relatively high abundances of these cell-types were observed to be visually concordant with specific spatial domains (Figure 3B, C). TNKILC and stromal cells were each related to two different 3D spatial domains (4 total spatial domains), while these same cell-types were associated with two (TNKILC) and one (stromal) 2D spatial domains, respectively – thus the single 2D stromal domain was subdivided into two 3D stromal domains with different function. The top biological function pathways associated with these spatial domains elucidated through gene set enrichment analysis, are presented in Tables 2 and 3. The TNKILC 2D and 3D domains each represented similar phenomenon.

Table 3: Pathway analysis results for 3D and 2D TNKILC domains.

3D TNKILC Domain A	**P-value**	**2D TNKILC Domain A**	**P-value**
Scavenging By Class F Receptors (R-HSA-3000484)	3.0e-3	Scavenging By Class F Receptors (R-HSA-3000484)	3.0e-3
HSF1 Activation (R-HSA-3371511)	1.4e-2	eNOS Activation (R-HSA-203615)	5.5e-3
mRNA Capping (R-HSA-72086)	1.6e-2	Attenuation Phase (R-HSA-3371568)	1.3e-2
3D TNKILC Domain B		**2D TNKILC Domain B**	
Cellular Response To Chemical Stress (R-HSA-9711123)	3.5e-3	Signaling By Rho GTPases (R-HSA-194315)	7.5e-6
Killing Mechanisms (R-HSA-9664420)	5.5e-3	Killing Mechanisms (R-HSA-9664420)	1.2e-5
Innate Immune System (R-HSA-168249)	6.2e-3	Immune System (R-HSA-168256)	1.2e-4

4. Discussion

3D ST can herald the transition to a more comprehensive representation of complex tissue volumes rather than 2D sections. We present the first study to investigate tumor heterogeneity using 3D ST inferred from routine histopathology with deep learning. Our

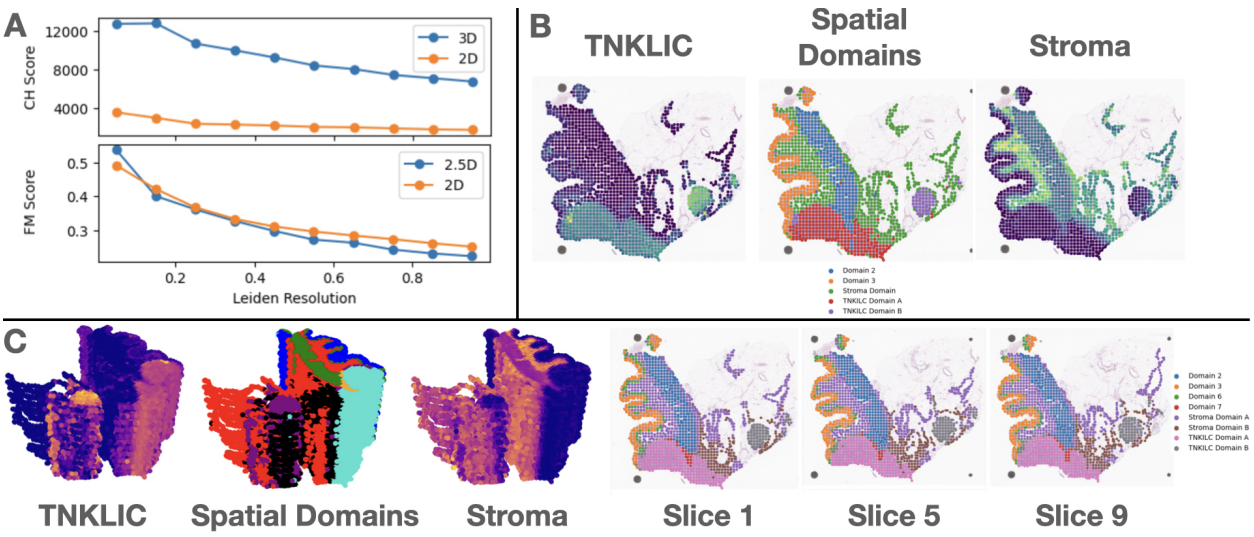

Figure 3: **A.** Spatial domain clustering quality measured through cluster separation and density, as well as agreement with groundtruth pathology annotations. **B.** Concordance of spatial domains with high abundance of TNKILC and stroma cells in tested 2D examples, and **C.** in 3D examples, visualized as complete 3D model as well as individual slices from the 3D model.

results demonstrate that inferred 3D ST can enhance spatial domain identification compared to typical 2D analyses, and that projection of this 3D information is capable of rendering a more nuanced interpretation of the TME through subdivision of cell-type associated domains.

In our experiments, 3D ST consistently identified a higher number of spatial domains compared to 2D approaches. This outcome suggests that incorporating multiple 2D transcriptomics sections to generate 3D ST data does not result in merely redundant information, even when the total sectioning depth is limited, as was necessary in this study due to the clinical use of tissue blocks. Unlike many other 3D studies that fully deplete the tissue block, our approach demonstrated that even with a shallower sectioning depth, 3D ST can reveal additional and distinct spatial domains. This underscores its utility in capturing more comprehensive and unique spatial information within each section, which, in turn, leads to the identification of a greater number of total biological domains. 3D spatial domain further resulted in greater clustering quality. These findings align with existing works demonstrating that considering multiple stacked 2D sections leads to superior spatial domain stratification (Dong and Zhang). However, our work is the first to demonstrate this premise using ST data generated through deep learning on routine imaging rather than costly sequencing-based ST assays. Such an approach can facilitate rapid generation of 3D ST data which may be used to inform selection of specimens prior to further costly lab-based processing. Alternatively, deep learning-based 3D ST generation may enable utilization of this data modality for biomarker discovery in resource-constrained settings where laboratory processing is infeasible.

Our results further showcase how 3D ST can elucidate prognostically relevant cell-type distribution in tissue volumes. We demonstrated that spatial domains captured further nuanced lineage specific pathways, hinting at potential for more granular molecular dissection of the tissue. For instance, in a prior study which explored 3D reconstruction of the skin, T cell distribution was found to be more proximal to helper T-cells when considering 3D structure as compared to 2D (Ghose et al.).

In our study, for stromal cells, gene signatures defining 3D Stromal Domain A appeared to related to pathways attributed to cancer associated fibroblasts (CAFs), evidenced by association with lipid reprograming as colorectal cancer as CAFs undergo metabolic reprogramming to accumulate and metabolize lipids (Gong et al.), cholesterol biosynthesis as they activate higher cholesterol uptake (Neuwirt

et al.), and elastic fibres as these have been found to be secreted by CAFs (Zhao et al.). 3D Stromal Domain B appeared to reflect macrophage activity, evidenced by consistent association with necrosis as a key macrophage function (Brouckaert et al.). The 2D Stromal Domain was associated with more fundamental pathways tied to zinc transport (Chen et al.), which have been hypothesized to be tied to chemoresistance mediated through stromal cells. Consistent association with NOTCH3, and toll-like receptors (TLRs) may indicate presence of macrophages (Thomas et al.; Serra et al.; Huang et al.) just as 3D Domain #2, though the single 2D Domain prevented further delineation of these effects.

For TNKILC cells, 3D TNKILC Domain A may localize NK and T cells, as Class F receptors commonly interact with NK cells (Goodridge et al.), and genes responsible for mRNA capping are upregulated following T cell activation (Galloway and Cowling). 3D TNKILC Domain B likely identified innate lymphoid cells (ILCs), as stress signals are responsible for ILC activation (Nagasawa et al.), and ILCs are part of the innate immune system. 2D TNKILC Domain A may localize NK and T cells through association with Class F receptors and eNOS which regulates T cell activation (Ibiza et al.). However, 2D TNKILC Domain B may also localize T cells as Rho GTPases are active in T cell regulation (Ahmad Mokhtar et al.). Thus, 2D domains are unable to pinpoint specific subtypes of TNKILC cells with the same granularity as 3D.

Overall, we concluded that 3D spatial domain localization of prognostically relevant cell subtypes was more granular and biologically significant than 2D spatial domains. This underscores the potential of 3D ST to reveal a higher number of spatial domains and provide a deeper understanding of tumor heterogeneity. While our study demonstrates the feasibility of using image-based deep learning for this purpose, future research can leverage 3D ST data to uncover specific biological insights that remain hidden in 2D analyses.

The primary limitation of this study was the restricted depth to which 3D tissue blocks were profiled. Due to institutional concerns about specimen preservation—since these were clinical blocks—we were limited to cutting only 10 five-micron sections per block, resulting in a total depth of approximately 70-100 microns. This constraint reduced the vertical resolution of our 3D models. Typically, blocks dedicated to clinical research rather than clinical use allow for more extensive sectioning, often involving bisecting the tissue or dissecting adjacent tissue for research-use biobanking. We anticipate that additional sectioning to enable a more comprehensive 3D examination of the specimen, or the use of other nondestructive 3D pathology imaging methods, would further elucidate the advantages of our approach. In the future, it will be important to consider that the optimal sectioning depth to maximize clinical relevance depends on tissue type and tumor characteristics such as invasive depth and section orientation. Our study was also limited by the set of 1000 genes for which we inferred ST expression. Sequencing-based ST data can encompass expression levels for more than 10,000 genes. While we anticipate that most of the accurately predicted biological pathways will be closely tied to histological features, we also expect variability in the predictiveness of different pathways. Understanding these differences will be an important focus of future research, potentially enabling the localization of more granular cell types and histological structures in 3D.

5. Conclusion

We present a proof-of-concept exploration of CRC tumor heterogeneity using 3D ST inferred from routine tissue imaging as means to study biomolecular structures reflecting the TME at scale. Our results indicate that 3D ST can represent the molecular heterogeneity of tumors with improved power compared to 2D analyses and may soon be used to facilitate fine-grained investigation of prognostically relevant biomarkers. This work opens the door to future efforts to explore inferred 3D ST data from histopathology with larger cohorts, with greater depth to reveal nuanced 3D architectures, which can be further enhanced through development of computational approaches adapted to 3D.

6. Funding and Acknowledgements

HK and KL are supported by NIH grant DK103831. JL is supported by Department of Defense grant PR220927, and NIH awards P20GM130454, P20GM104416, R24GM141194, R01CA277810.

References

Ana Masara Ahmad Mokhtar, Nor Hawani Salikin, Aminah Suhaila Haron, Syafinaz Amin-Nordin,

Ilie Fadzilah Hashim, Muaz Mohd Zaini Makhtar, Siti Balqis Zulfigar, and Nurul Izza Ismail. RhoG's role in t cell activation and function. 13:845064. ISSN 1664-3224. doi: 10.3389/fimmu.2022.845064. URL https://www.frontiersin.org/articles/10.3389/fimmu.2022.845064/full.

Greet Brouckaert, Michael Kalai, Dmitri V. Krysko, Xavier Saelens, Dominique Vercammen, 'Matladi Ndlovu, Guy Haegeman, Katharina D'Herde, and Peter Vandenabeele. Phagocytosis of necrotic cells by macrophages is phosphatidylserine dependent and does not induce inflammatory cytokine production. 15(3):1089–1100. ISSN 1059-1524, 1939-4586. doi: 10.1091/mbc.e03-09-0668. URL https://www.molbiolcell.org/doi/10.1091/mbc.e03-09-0668.

T. Calinski and J. Harabasz. A dendrite method for cluster analysis. 3(1):1–27. ISSN 0361-0926. doi: 10.1080/03610927408827101. URL http://www.tandfonline.com/doi/abs/10.1080/03610927408827101.

Bonan Chen, Peiyao Yu, Wai Nok Chan, Fuda Xie, Yigan Zhang, Li Liang, Kam Tong Leung, Kwok Wai Lo, Jun Yu, Gary M. K. Tse, Wei Kang, and Ka Fai To. Cellular zinc metabolism and zinc signaling: from biological functions to diseases and therapeutic targets. 9(1):6. ISSN 2059-3635. doi: 10.1038/s41392-023-01679-y. URL https://www.nature.com/articles/s41392-023-01679-y.

Ibiayi Dagogo-Jack and Alice T. Shaw. Tumour heterogeneity and resistance to cancer therapies. 15(2):81–94. ISSN 1759-4774, 1759-4782. doi: 10.1038/nrclinonc.2017.166. URL https://www.nature.com/articles/nrclinonc.2017.166.

Kangning Dong and Shihua Zhang. Deciphering spatial domains from spatially resolved transcriptomics with an adaptive graph attention auto-encoder. 13(1):1739. ISSN 2041-1723. doi: 10.1038/s41467-022-29439-6. URL https://www.nature.com/articles/s41467-022-29439-6.

Michael Fatemi, Eric Feng, Cyril Sharma, Zarif Azher, Tarushii Goel, Ojas Ramwala, Scott M. Palisoul, Rachael E. Barney, Laurent Perreard, Fred W. Kolling, Lucas A. Salas, Brock C. Christensen, Gregory J. Tsongalis, Louis J. Vaickus, and Joshua J. Levy. Inferring spatial transcriptomics markers from whole slide images to characterize metastasis-related spatial heterogeneity of colorectal tumors: A pilot study. 14: 100308. ISSN 21533539. doi: 10.1016/j.jpi.2023.100308. URL https://linkinghub.elsevier.com/retrieve/pii/S2153353923001220.

E. B. Fowlkes and C. L. Mallows. A method for comparing two hierarchical clusterings. 78 (383):553–569. ISSN 0162-1459, 1537-274X. doi: 10.1080/01621459.1983.10478008. URL http://www.tandfonline.com/doi/abs/10.1080/01621459.1983.10478008.

Alison Galloway and Victoria H. Cowling. mRNA cap regulation in mammalian cell function and fate. 1862(3):270–279. ISSN 18749399. doi: 10.1016/j.bbagrm.2018.09.011. URL https://linkinghub.elsevier.com/retrieve/pii/S1874939918301676.

Chandler D. Gatenbee, Ann-Marie Baker, Sandhya Prabhakaran, Ottilie Swinyard, Robbert J. C. Slebos, Gunjan Mandal, Eoghan Mulholland, Noemi Andor, Andriy Marusyk, Simon Leedham, Jose R. Conejo-Garcia, Christine H. Chung, Mark Robertson-Tessi, Trevor A. Graham, and Alexander R. A. Anderson. Virtual alignment of pathology image series for multi-gigapixel whole slide images. 14(1):4502. ISSN 2041-1723. doi: 10.1038/s41467-023-40218-9. URL https://www.nature.com/articles/s41467-023-40218-9.

Soumya Ghose, Yingnan Ju, Elizabeth McDonough, Jonhan Ho, Arivarasan Karunamurthy, Chrystal Chadwick, Sanghee Cho, Rachel Rose, Alex Corwin, Christine Surrette, Jessica Martinez, Eric Williams, Anup Sood, Yousef Al-Kofahi, Louis D. Falo, Katy Börner, and Fiona Ginty. 3d reconstruction of skin and spatial mapping of immune cell density, vascular distance and effects of sun exposure and aging. 6(1):718. ISSN 2399-3642. doi: 10.1038/s42003-023-04991-z. URL https://www.nature.com/articles/s42003-023-04991-z.

Adam K. Glaser, Nicholas P. Reder, Ye Chen, Chengbo Yin, Linpeng Wei, Soyoung Kang, Lindsey A. Barner, Weisi Xie, Erin F. McCarty, Chenyi Mao, Aaron R. Halpern, Caleb R. Stoltzfus, Jonathan S. Daniels, Michael Y. Gerner, Philip R. Nicovich, Joshua C. Vaughan, Lawrence D. True, and Jonathan T. C. Liu. Multi-immersion open-top light-sheet microscope for high-throughput imaging of cleared tissues.

10(1):2781. ISSN 2041-1723. doi: 10.1038/s41467-019-10534-0. URL https://www.nature.com/articles/s41467-019-10534-0.

Jin Gong, Yiyun Lin, Huaqin Zhang, Chunqi Liu, Zhong Cheng, Xiaowei Yang, Jiamei Zhang, Yuanyuan Xiao, Na Sang, Xinying Qian, Liang Wang, Xiaobo Cen, Xiao Du, and Yinglan Zhao. Reprogramming of lipid metabolism in cancer-associated fibroblasts potentiates migration of colorectal cancer cells. 11(4):267. ISSN 2041-4889. doi: 10.1038/s41419-020-2434-z. URL https://www.nature.com/articles/s41419-020-2434-z.

Jodie P. Goodridge, Aura Burian, Ni Lee, and Daniel E. Geraghty. HLA-f and MHC class i open conformers are ligands for NK cell ig-like receptors. 191(7):3553–3562. ISSN 0022-1767, 1550-6606. doi: 10.4049/jimmunol.1300081. URL https://journals.aai.org/jimmunol/article/191/7/3553/39876/HLA-F-and-MHC-Class-I-Open-Conformers-Are-Ligands.

Kai Huang, Wenwu Luo, Jinmei Fang, Changjun Yu, Guangjie Liu, Xiaodong Yuan, Yun Liu, and Wenyong Wu. Notch3 signaling promotes colorectal tumor growth by enhancing immunosuppressive cells infiltration in the microenvironment. 23(1):55. ISSN 1471-2407. doi: 10.1186/s12885-023-10526-w. URL https://bmccancer.biomedcentral.com/articles/10.1186/s12885-023-10526-w.

Sales Ibiza, Víctor M. Víctor, Irene Boscá, Angel Ortega, Ana Urzainqui, José E. O'Connor, Francisco Sánchez-Madrid, Juan V. Esplugues, and Juan M. Serrador. Endothelial nitric oxide synthase regulates t cell receptor signaling at the immunological synapse. 24(6):753–765. ISSN 10747613. doi: 10.1016/j.immuni.2006.04.006. URL https://linkinghub.elsevier.com/retrieve/pii/S1074761306002640.

Maxim V. Kuleshov, Matthew R. Jones, Andrew D. Rouillard, Nicolas F. Fernandez, Qiaonan Duan, Zichen Wang, Simon Koplev, Sherry L. Jenkins, Kathleen M. Jagodnik, Alexander Lachmann, Michael G. McDermott, Caroline D. Monteiro, Gregory W. Gundersen, and Avi Ma'ayan. Enrichr: a comprehensive gene set enrichment analysis web server 2016 update. 44:W90–W97. ISSN 0305-1048, 1362-4962. doi: 10.1093/nar/gkw377. URL https://academic.oup.com/nar/article-lookup/doi/10.1093/nar/gkw377.

Alona Levy-Jurgenson, Xavier Tekpli, Vessela N. Kristensen, and Zohar Yakhini. Spatial transcriptomics inferred from pathology whole-slide images links tumor heterogeneity to survival in breast and lung cancer. 10(1):18802. ISSN 2045-2322. doi: 10.1038/s41598-020-75708-z. URL https://www.nature.com/articles/s41598-020-75708-z.

Jia-Ren Lin, Shu Wang, Shannon Coy, Yu-An Chen, Clarence Yapp, Madison Tyler, Maulik K. Nariya, Cody N. Heiser, Ken S. Lau, Sandro Santagata, and Peter K. Sorger. Multiplexed 3d atlas of state transitions and immune interaction in colorectal cancer. 186(2):363–381.e19. ISSN 00928674. doi: 10.1016/j.cell.2022.12.028. URL https://linkinghub.elsevier.com/retrieve/pii/S0092867422015719.

Jonathan T. C. Liu, Adam K. Glaser, Kaustav Bera, Lawrence D. True, Nicholas P. Reder, Kevin W. Eliceiri, and Anant Madabhushi. Harnessing non-destructive 3d pathology. 5(3):203–218. ISSN 2157-846X. doi: 10.1038/s41551-020-00681-x. URL https://www.nature.com/articles/s41551-020-00681-x.

Romain Lopez, Jeffrey Regier, Michael B. Cole, Michael I. Jordan, and Nir Yosef. Deep generative modeling for single-cell transcriptomics. 15(12):1053–1058. ISSN 1548-7091, 1548-7105. doi: 10.1038/s41592-018-0229-2. URL https://www.nature.com/articles/s41592-018-0229-2.

Fabiana Lüönd, Stefanie Tiede, and Gerhard Christofori. Breast cancer as an example of tumour heterogeneity and tumour cell plasticity during malignant progression. 125(2):164–175. ISSN 0007-0920, 1532-1827. doi: 10.1038/s41416-021-01328-7. URL https://www.nature.com/articles/s41416-021-01328-7.

Marc Macenko, Marc Niethammer, J. S. Marron, David Borland, John T. Woosley, Xiaojun Guan, Charles Schmitt, and Nancy E. Thomas. A method for normalizing histology slides for quantitative analysis. In *2009 IEEE International Symposium on Biomedical Imaging: From Nano to Macro*, pages 1107–1110. IEEE. ISBN 978-1-4244-3931-7. doi: 10.1109/ISBI.2009.5193250. URL http://ieeexplore.ieee.org/document/5193250/.

Leland McInnes, John Healy, Nathaniel Saul, and Lukas Großberger. UMAP: Uniform manifold approximation and projection. 3(29):861. ISSN 2475-9066. doi: 10.21105/joss.00861. URL http://joss.theoj.org/papers/10.21105/joss.00861.

Marija Milacic, Deidre Beavers, Patrick Conley, Chuqiao Gong, Marc Gillespie, Johannes Griss, Robin Haw, Bijay Jassal, Lisa Matthews, Bruce May, Robert Petryszak, Eliot Ragueneau, Karen Rothfels, Cristoffer Sevilla, Veronica Shamovsky, Ralf Stephan, Krishna Tiwari, Thawfeek Varusai, Joel Weiser, Adam Wright, Guanming Wu, Lincoln Stein, Henning Hermjakob, and Peter D'Eustachio. The reactome pathway knowledgebase 2024. 52: D672–D678. ISSN 0305-1048, 1362-4962. doi: 10.1093/nar/gkad1025. URL https://academic.oup.com/nar/article/52/D1/D672/7369850.

Chiara Molinari, Giorgia Marisi, Alessandro Passardi, Laura Matteucci, Giulia De Maio, and Paola Ulivi. Heterogeneity in colorectal cancer: A challenge for personalized medicine? 19(12):3733. ISSN 1422-0067. doi: 10.3390/ijms19123733. URL https://www.mdpi.com/1422-0067/19/12/3733.

Eileen Morgan, Melina Arnold, A Gini, V Lorenzoni, C J Cabasag, Mathieu Laversanne, Jerome Vignat, Jacques Ferlay, Neil Murphy, and Freddie Bray. Global burden of colorectal cancer in 2020 and 2040: incidence and mortality estimates from GLOBOCAN. 72(2):338–344. ISSN 0017-5749, 1468-3288. doi: 10.1136/gutjnl-2022-327736. URL https://gut.bmj.com/lookup/doi/10.1136/gutjnl-2022-327736.

Maho Nagasawa, Hergen Spits, and Xavier Romero Ros. Innate lymphoid cells (ILCs): Cytokine hubs regulating immunity and tissue homeostasis. 10(12):a030304. ISSN 1943-0264. doi: 10.1101/cshperspect.a030304. URL http://cshperspectives.cshlp.org/lookup/doi/10.1101/cshperspect.a030304.

Hannes Neuwirt, Jan Bouchal, Gvantsa Kharaishvili, Christian Ploner, Karin Jöhrer, Florian Pitterl, Anja Weber, Helmut Klocker, and Iris E. Eder. Cancer-associated fibroblasts promote prostate tumor growth and progression through upregulation of cholesterol and steroid biosynthesis. 18(1):11. ISSN 1478-811X. doi: 10.1186/s12964-019-0505-5. URL https://biosignaling.biomedcentral.com/articles/10.1186/s12964-019-0505-5.

Karin Pelka, Matan Hofree, Jonathan H. Chen, Siranush Sarkizova, Joshua D. Pirl, Vjola Jorgji, Alborz Bejnood, Danielle Dionne, William H. Ge, Katherine H. Xu, Sherry X. Chao, Daniel R. Zollinger, David J. Lieb, Jason W. Reeves, Christopher A. Fuhrman, Margaret L. Hoang, Toni Delorey, Lan T. Nguyen, Julia Waldman, Max Klapholz, Isaac Wakiro, Ofir Cohen, Julian Albers, Christopher S. Smillie, Michael S. Cuoco, Jingyi Wu, Mei-ju Su, Jason Yeung, Brinda Vijaykumar, Angela M. Magnuson, Natasha Asinovski, Tabea Moll, Max N. Goder-Reiser, Anise S. Applebaum, Lauren K. Brais, Laura K. DelloStritto, Sarah L. Denning, Susannah T. Phillips, Emma K. Hill, Julia K. Meehan, Dennie T. Frederick, Tatyana Sharova, Abhay Kanodia, Ellen Z. Todres, Judit Jané-Valbuena, Moshe Biton, Benjamin Izar, Conner D. Lambden, Thomas E. Clancy, Ronald Bleday, Nelya Melnitchouk, Jennifer Irani, Hiroko Kunitake, David L. Berger, Amitabh Srivastava, Jason L. Hornick, Shuji Ogino, Asaf Rotem, Sébastien Vigneau, Bruce E. Johnson, Ryan B. Corcoran, Arlene H. Sharpe, Vijay K. Kuchroo, Kimmie Ng, Marios Giannakis, Linda T. Nieman, Genevieve M. Boland, Andrew J. Aguirre, Ana C. Anderson, Orit Rozenblatt-Rosen, Aviv Regev, and Nir Hacohen. Spatially organized multicellular immune hubs in human colorectal cancer. 184(18):4734–4752.e20. ISSN 00928674. doi: 10.1016/j.cell.2021.08.003. URL https://linkinghub.elsevier.com/retrieve/pii/S0092867421009454.

Marie Schott, Daniel León-Periñán, Elena Splendiani, Leon Strenger, Jan Robin Licha, Tancredi Massimo Pentimalli, Simon Schallenberg, Jonathan Alles, Sarah Samut Tagliaferro, Anastasiya Boltengagen, Sebastian Ehrig, Stefano Abbiati, Steffen Dommerich, Massimiliano Pagani, Elisabetta Ferretti, Giuseppe Macino, Nikos Karaiskos, and Nikolaus Rajewsky. Open-ST: High-resolution spatial transcriptomics in 3d. 187(15):3953–3972.e26. ISSN 00928674. doi: 10.1016/j.cell.2024.05.055. URL https://linkinghub.elsevier.com/retrieve/pii/S0092867424006366.

Marina Serra, Amedeo Columbano, Ummi Ammarah, Massimiliano Mazzone, and Alessio Menga. Understanding metal dynamics between cancer cells and macrophages: Competition or synergism? 10: 646. ISSN 2234-943X. doi: 10.3389/fonc.2020.

00646. URL https://www.frontiersin.org/article/10.3389/fonc.2020.00646/full.

Gokul Srinivasan, Zarif Azher, Michael Fatemi, and Joshua J. Levy. Development and large scale validation of deep learning for colorectal cancer spatial transcriptomics inference from routine histopathology.

Valentine Svensson, Sarah A Teichmann, and Oliver Stegle. SpatialDE: identification of spatially variable genes. 15(5):343–346. ISSN 1548-7091, 1548-7105. doi: 10.1038/nmeth.4636. URL https://www.nature.com/articles/nmeth.4636.

Graham Thomas, Luca Micci, Wenjing Yang, Joseph Katakowski, Cecilia Oderup, Purnima Sundar, Xiao Wang, Kenneth G. Geles, Shobha Potluri, and Shahram Salek-Ardakani. Intratumoral activation of endosomal TLR pathways reveals a distinct role for TLR3 agonist dependent type-1 interferons in shaping the tumor immune microenvironment. 11:711673. ISSN 2234-943X. doi: 10.3389/fonc.2021.711673. URL https://www.frontiersin.org/articles/10.3389/fonc.2021.711673/full.

Luyi Tian, Fei Chen, and Evan Z. Macosko. The expanding vistas of spatial transcriptomics. 41 (6):773–782. ISSN 1087-0156, 1546-1696. doi: 10.1038/s41587-022-01448-2. URL https://www.nature.com/articles/s41587-022-01448-2.

V. A. Traag, L. Waltman, and N. J. Van Eck. From louvain to leiden: guaranteeing well-connected communities. 9(1):5233. ISSN 2045-2322. doi: 10.1038/s41598-019-41695-z. URL https://www.nature.com/articles/s41598-019-41695-z.

Sanja Vickovic, Denis Schapiro, Konstantin Carlberg, Britta Lötstedt, Ludvig Larsson, Franziska Hildebrandt, Marina Korotkova, Aase H. Hensvold, Anca I. Catrina, Peter K. Sorger, Vivianne Malmström, Aviv Regev, and Patrik L. Ståhl. Three-dimensional spatial transcriptomics uncovers cell type localizations in the human rheumatoid arthritis synovium. 5(1):129. ISSN 2399-3642. doi: 10.1038/s42003-022-03050-3. URL https://www.nature.com/articles/s42003-022-03050-3.

Gefei Wang, Jia Zhao, Yan Yan, Yang Wang, Angela Ruohao Wu, and Can Yang. Construction of a 3d whole organism spatial atlas by joint modelling of multiple slices with deep neural networks. 5(11):1200–1213, a. ISSN 2522-5839. doi: 10.1038/s42256-023-00734-1. URL https://www.nature.com/articles/s42256-023-00734-1.

Mingyue Wang, Qinan Hu, Tianhang Lv, Yuhang Wang, Qing Lan, Rong Xiang, Zhencheng Tu, Yanrong Wei, Kai Han, Chang Shi, Junfu Guo, Chao Liu, Tao Yang, Wensi Du, Yanru An, Mengnan Cheng, Jiangshan Xu, Haorong Lu, Wangsheng Li, Shaofang Zhang, Ao Chen, Wei Chen, Yuxiang Li, Xiaoshan Wang, Xun Xu, Yuhui Hu, and Longqi Liu. High-resolution 3d spatiotemporal transcriptomic maps of developing drosophila embryos and larvae. 57(10):1271–1283.e4, b. ISSN 15345807. doi: 10.1016/j.devcel.2022.04.006. URL https://linkinghub.elsevier.com/retrieve/pii/S1534580722002465.

Mingyue Wang, Qinan Hu, Tianhang Lv, Yuhang Wang, Qing Lan, Rong Xiang, Zhencheng Tu, Yanrong Wei, Kai Han, Chang Shi, Junfu Guo, Chao Liu, Tao Yang, Wensi Du, Yanru An, Mengnan Cheng, Jiangshan Xu, Haorong Lu, Wangsheng Li, Shaofang Zhang, Ao Chen, Wei Chen, Yuxiang Li, Xiaoshan Wang, Xun Xu, Yuhui Hu, and Longqi Liu. High-resolution 3d spatiotemporal transcriptomic maps of developing drosophila embryos and larvae. 57(10):1271–1283.e4, c. ISSN 15345807. doi: 10.1016/j.devcel.2022.04.006. URL https://linkinghub.elsevier.com/retrieve/pii/S1534580722002465.

Lisa N. Waylen, Hieu T. Nim, Luciano G. Martelotto, and Mirana Ramialison. From whole-mount to single-cell spatial assessment of gene expression in 3d. 3(1):602. ISSN 2399-3642. doi: 10.1038/s42003-020-01341-1. URL https://www.nature.com/articles/s42003-020-01341-1.

Weisi Xie, Nicholas P. Reder, Can Koyuncu, Patrick Leo, Sarah Hawley, Hongyi Huang, Chenyi Mao, Nadia Postupna, Soyoung Kang, Robert Serafin, Gan Gao, Qinghua Han, Kevin W. Bishop, Lindsey A. Barner, Pingfu Fu, Jonathan L. Wright, C. Dirk Keene, Joshua C. Vaughan, Andrew Janowczyk, Adam K. Glaser, Anant Madabhushi, Lawrence D. True, and Jonathan T.C. Liu. Prostate cancer risk stratification via nondestructive 3d pathology with deep learning–assisted gland analysis. 82(2):334–345. ISSN 0008-5472, 1538-7445. doi: 10.1158/0008-5472.CAN-21-2843. URL https://aacrjournals.

org/cancerres/article/82/2/334/675486/Prostate-Cancer-Risk-Stratification-via.

Yuansong Zeng, Zhuoyi Wei, Weijiang Yu, Rui Yin, Yuchen Yuan, Bingling Li, Zhonghui Tang, Yutong Lu, and Yuedong Yang. Spatial transcriptomics prediction from histology jointly through transformer and graph neural networks. 23(5):bbac297. ISSN 1467-5463, 1477-4054. doi: 10.1093/bib/bbac297. URL https://academic.oup.com/bib/article/doi/10.1093/bib/bbac297/6645485.

Zehua Zhao, Tianming Li, Yuan Yuan, and Yanmei Zhu. What is new in cancer-associated fibroblast biomarkers? 21(1):96. ISSN 1478-811X. doi: 10.1186/s12964-023-01125-0. URL https://biosignaling.biomedcentral.com/articles/10.1186/s12964-023-01125-0.

Ziwen Zheng, Thomas Wieder, Bernhard Mauerer, Luisa Schäfer, Rebecca Kesselring, and Heidi Braumüller. T cells in colorectal cancer: Unravelling the function of different t cell subsets in the tumor microenvironment. 24(14):11673. ISSN 1422-0067. doi: 10.3390/ijms241411673. URL https://www.mdpi.com/1422-0067/24/14/11673.

Yuan Zhou, Shuhui Bian, Xin Zhou, Yueli Cui, Wendong Wang, Lu Wen, Limei Guo, Wei Fu, and Fuchou Tang. Single-cell multiomics sequencing reveals prevalent genomic alterations in tumor stromal cells of human colorectal cancer. 38(6):818–828.e5. ISSN 15356108. doi: 10.1016/j.ccell.2020.09.015. URL https://linkinghub.elsevier.com/retrieve/pii/S153561082030489X.

Appendix A.

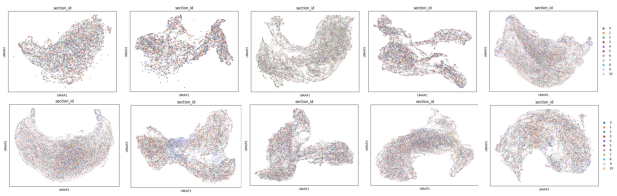

Figure 4: Examples of spatial domains identified in 3D tumor models across tested clustering resolutions.